Combustion Science and Technology
Publication details, including instructions for authors and subscription information:
http://www.tandfonline.com/loi/gcst20

Temperature Response of an Acoustically Forced Turbulent Lean Premixed Flame: A Quantitative Experimental Determination

Robin S. M. Chrystie [a], Iain S. Burns [b] & Clemens F. Kaminski [c]

[a] Clean Combustion Research Centre, King Abdullah University of Science and Technology, Jeddah, Saudi Arabia

[b] Department of Chemical and Process Engineering, University of Strathclyde, Glasgow, UK

[c] Department of Chemical Engineering and Biotechnology, University of Cambridge, Cambridge, UK

Accepted author version posted online: 19 Jul 2012.Published online: 16 Jan 2013.

To cite this article: Robin S. M. Chrystie , Iain S. Burns & Clemens F. Kaminski (2013) Temperature Response of an Acoustically Forced Turbulent Lean Premixed Flame: A Quantitative Experimental Determination, Combustion Science and Technology, 185:1, 180-199, DOI: 10.1080/00102202.2012.714020

To link to this article: http://dx.doi.org/10.1080/00102202.2012.714020

Combust. Sci. Technol., 185: 180–199, 2013

ISSN: 0010-2202 print/1563-521X online
DOI: 10.1080/00102202.2012.714020

Taylor & Francis
Taylor & Francis Group

TEMPERATURE RESPONSE OF AN ACOUSTICALLY FORCED TURBULENT LEAN PREMIXED FLAME: A QUANTITATIVE EXPERIMENTAL DETERMINATION

Robin S. M. Chrystie,[1] Iain S. Burns,[2] and Clemens F. Kaminski[3]

[1]*Clean Combustion Research Centre, King Abdullah University of Science and Technology, Jeddah, Saudi Arabia*

[2]*Department of Chemical and Process Engineering, University of Strathclyde, Glasgow, UK*

[3]*Department of Chemical Engineering and Biotechnology, University of Cambridge, Cambridge, UK*

Temperature measurements have been taken on an acoustically forced lean premixed turbulent bluff-body stabilized flame. The burner used in this study is a test-bed to investigate thermoacoustic instability in gas-turbine engines at the University of Cambridge. Numerous experiments have been performed on the burner, one of which used two-line OH planar laser induced fluorescence to measure temperature. Here, we employ vibrational coherent anti-Stokes Raman scattering (CARS) of nitrogen as an alternative to measure temperature, circumventing the limitations of the former method. The use of nitrogen CARS avoids the problem of probing regions of the flame with low OH concentrations that resulted in erroneous temperature. Such an application of CARS showed that the results from previous efforts were systematically biased up to 47% close to the bluff-body. We also critically review the limitations of CARS used in our experiments, pertaining to spatial resolution and associated biasing further downstream from the bluff-body. Using the more accurate results from this work, more up-to-date computational fluid dynamical (CFD) models of the burner can be validated, with the aim of improved understanding and prediction of thermoacoustic instability in gas turbines.

Keywords: Combustion; Flame instability; Gas turbines; Lasers; Lean mixture; Temperature measurement

INTRODUCTION

Lean premixed combustion is considered a viable option for reducing nitrous oxide emissions in gas turbine engines. However, this combustion regime can suffer from spontaneous fluctuation of the flame, and such instability in these engines is referred to as thermoacoustic oscillation. The global mechanism behind thermoacoustic oscillation is based on the positive feedback between heat release fluctuation

Received 16 February 2012; revised 29 June 2012; accepted 17 July 2012.

Address correspondence to Robin S. M. Chrystie, Clean Combustion Research Centre, King Abdullah University of Science and Technology, Jeddah 23955-6900, Saudi Arabia. E-mail: robin.chrystie@cantab.net

(q') from unsteady combustion and the associated combustion induced pressure oscillations (p') of the system (Dowling, 2000b). The necessary condition for such instability to occur is governed by the Rayleigh criterion (Lieuwen et al., 1998) and is readily satisfied in the lean premixed regime. The source term in the Rayleigh criterion is defined by the product of q' and p', in which the phase difference between these two variables is determined by a sequence of more elementary driving mechanisms. The criterion is useful for interpreting experimental data and identifying these driving mechanisms; such mechanisms need to be identified to predict and control occurrences of instability.

An example driving mechanism that forms the basis of this study is based on coherent vortices that can be generated by velocity perturbations or obstacles present in the flow such as flame holders. Such vortices, when convected downstream, impinge on the flame. This in turn leads to unsteady combustion, and hence unsteady heat release rate. This process can promote self-excited oscillation of the flame with amplitude that grows in time until a limit cycle is established. The amplitude of the temperature and pressure oscillations can become sufficiently large that structural damage of the combustor ensues, in addition to the risk of sudden global extinction of the flame.

Major research activity is ongoing internationally in an effort to generate tools whereby this form of combustion instability can be better understood, predicted, and prevented. These efforts are usually based on computational fluid dynamical (CFD) models of model burners. Temperature is a key determinant in the onset and maintenance of thermoacoustic instability, since the heat release from the flame drives the oscillation and is highly temperature dependent (Dowling, 2000a). Temperature is thus a key variable in CFD models, and comparison to experimental data allows validation of assumptions within those models. Although we use a simple model burner in this research, the work can be seen in the larger context of lean premixed prevaporized (LPP) gas turbine technology (Bauer, 2004). Phenomena observed here on a laboratory scale add insight into unsteady combustion in such real-world combustors. Using a representative model burner, we can study the fundamental mechanics of this phenomenon for its control and prevention.

Thus far, extensive research has been done to study turbulent flame phenomena in relation to a model burner (e.g., Ahmed et al., 2007; Armitage et al., 2006; Ayache et al., 2010; Ayoola et al., 2009; Balachandran et al., 2005; Chrystie et al., 2008; Swaminathan et al., 2011). The purpose of the burner is to mimic the behavior of an industrial LPP combustor, which exhibits flame pulsation. It provides an experimental test bed for validation and development of CFD models of the flame. However, with ongoing development of CFD models, there is continuing demand for an up-to-date database of experimental variables such as species composition, reaction rates, flow-field velocities, and temperature.

The only CFD study performed on the model burner hitherto for this work used unsteady Reynolds averaged Navier–Stokes (URANS) code (Armitage et al., 2006). The code assumed adiabatic boundary conditions, which reduces computational complexity. Consequently, the code resulted in temperatures and flow-field velocities that were qualitative in nature. A manifestation of the imperfect boundary conditions is the slower rate of propagation of the vortex in the reactants that rolls up the flamefront during the acoustic cycle. The effect could be due to the adiabatic

wall condition, where "wall" here comprises the inner boundary of the encapsulating chamber surrounding the flame, and the surface of the bluff-body at the flame base. The adiabatic wall condition raises the overall temperature of the burned gases and increases their viscosity. This would hence retard the rate of vortex propagation through the more viscous burned gases. To overcome the effects of an unrealistic boundary condition, it is suggested that an alternative wall-function embedded within the Reynolds stress submodel could be developed as an improvement to the URANS code. The submodel can then be validated by comparing the resulting temperatures from the modified URANS code with an experimental database.

Nevertheless, an experimental database had been generated previously using two-line OH planar laser induced fluorescence (PLIF) (Ayoola et al., 2009) in an effort to validate the first modeling attempt employing the abovementioned URANS code (Armitage et al., 2006). However, limitations inherent to the technique also rendered the data to be somewhat qualitative. This was manifest in the temperatures of the region of the flame immediately above the bluff-body of the model burner, where the temperatures would be expected to be closer to the adiabatic limit of 1706 K (Morley, 1997) for an equivalence ratio of 0.55 used in this study. However, results from the OH PLIF technique yielded 900 K. It is plausible that the apparent cool region could be due to thermal conduction of heat to the metal bluff-body. Nonetheless, the amount of conduction seems excessive, owing to the extent of the cool region prevailing in the burned gases. This is allied with the finding that the thermal boundary layer thickness at the bluff-body, as estimated using correlations in Chrystie (2009b), is approximately an order of magnitude less than what the temperature profiles suggest.

In light of the above, the cool region in the burned gases is suspected to artificially stem from a possible systematic error in the two-line OH PLIF temperature measurement. One likely source is subtraction of either too much or too little background from the raw OH PLIF images during preprocessing of the raw data. This imperfect correction would affect the two-line temperature map, and more strongly in the regions corresponding to low OH fluorescence intensity (Chrystie, 2009b). It is considered here that the implementation of two-line OH PLIF to the model burner may not yield reliable temperatures in the burned gases when OH signals are low. Hence, in these circumstances, planar OH LIF may not deliver quantitative results, but is better suited to provide an instant image of the flame shape and behavior with time. An alternative technique to measure temperature is therefore needed if the results are to be used to validate a more up-to-date URANS models of the burner.

Two candidates offering improved accuracy include indium two-line atomic fluorescence (TLAF) and coherent anti-Stokes Raman scattering (CARS). Indium TLAF applied successfully by the group (Burns et al., 2011; Chrystie et al., 2009a; Hult et al., 2005) is a powerful thermometric technique due to its ability to measure rapid transients in temperature with precision and accuracy, along with high spatial and temporal resolution, and the added potential to capture temperature data in 2-D. Despite all the advantages of this technique, it would suffer from a key limitation for the flame type in this study: the conditions are too lean for there to be an abundant uniform distribution of indium probe species throughout the flame. In this article, we apply CARS as the best alternative, but it is a point measurement technique. Although CARS cannot provide information on the instantaneous flame

shape, it is accurate. Accuracy is greatly improved for the application of CARS in vibrationally excited nitrogen molecules. This is because of the abundance of nitrogen in lean fuel/air flames, where the concentration of nitrogen is high and approximately uniform throughout the flame. This overcomes the problem of potential susceptibility to error in temperature incurring from nonperfect background correction, as was the case in two-line OH PLIF when OH signals were low. This is the major motivation for the use of vibrational nitrogen CARS for the model burner, in order to acquire quantitative temperatures for the goal of validating URANS models. Furthermore, vibrational nitrogen CARS offers a better accuracy of about 1% at ~2000 K (Eckbreth and Hall, 1981), when compared to that of two-line OH PLIF, which offers an accuracy of about 5–10% under optimal conditions (i.e., in the absence of the problem of low OH concentrations) (Seitzman et al., 1994).

EXPERIMENTAL METHOD

Our method works in principle by taking point measurements throughout the axial cross-section of the flame. The cross-section is the same as previous studies on this burner. Point measurements were recorded by triggering an Nd:YAG laser to a phase-angle of the acoustic cycle, and then averaging the measurements over a number of cycles. This resulted in phase-averaged temperatures. This process was repeated over numerous points throughout the same cross-section to allow an interpolated map of phase-averaged temperature to be generated, which allows for a direct comparison to previously obtained phase-averaged temperature maps from the OH PLIF technique.

Burner Setup

The acoustically forced bluff-body burner used in this study is depicted by its central cross-section in Figure 1a. The 10 kW burner was supplied by a lean mixture of air and ethylene at an equivalence ratio of 0.55. The flow was acoustically forced by passing sinusoidal sound waves through the mixture, using a signal generator (TTi TGA 1242) and an 80 W preamplifier. The flow conditions described below originate from the work of Balachandran (2005) and Ayoola et al. (2009). A limited number of flow conditions could only be investigated in this work, owing to time constraints. This stems from the long time needed to record a sufficient number of temperatures, in order to generate interpolated temperature maps using CARS. Therefore, the parameters of the flow conditions were carefully selected, in order to acquire sufficient information about the evolution of the flame and its structure. One such parameter is the frequency of acoustic forcing, which was fixed at 160 Hz, corresponding to one of the axial resonant frequencies of the burner's plenum. This frequency is of interest, as it yields a large amplitude of oscillation in the flow for a given voltage applied to the speakers, owing to the resonant condition (Balachandran et al., 2005). The amplitude of oscillation was set to a ratio of $A = 0.65$ (expressed as half peak-to-peak amplitude in burner outlet gas velocity to time-averaged flow velocity). The time-averaged flow velocity corresponds to a Reynolds number, which is based on the cross-sectional area equivalent diameter of the burner exit, of $Re = 17{,}000$. This rate of flow resulted in a turbulent flame that was stabilized on the central

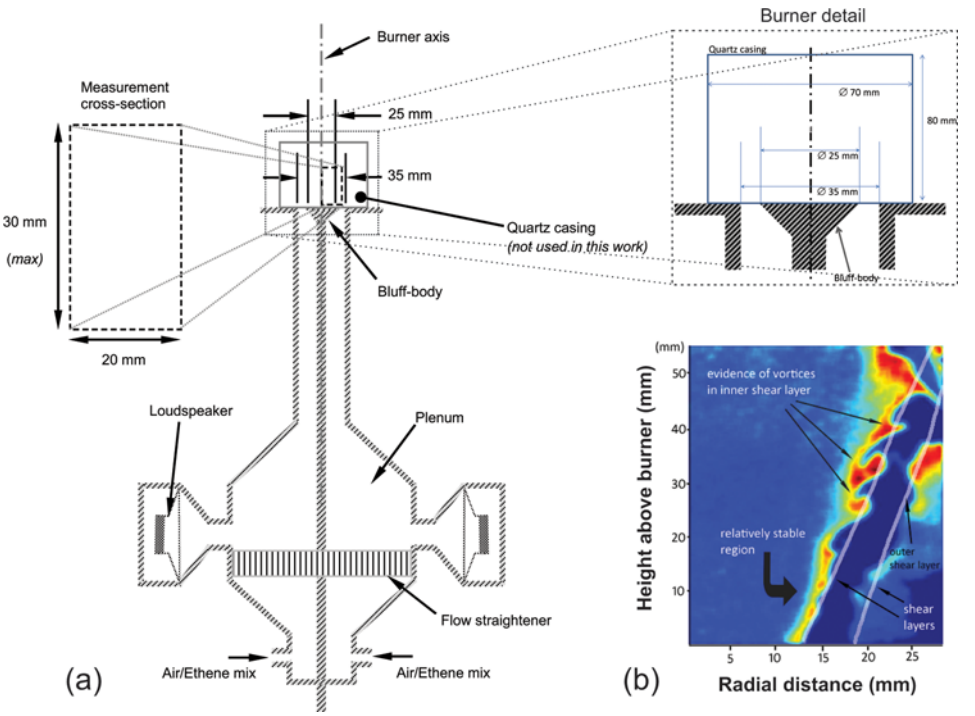

Figure 1 (a) Schematic of the acoustically forced bluff-body burner cross-section, with detail of the burner outlet. (b) Instantaneous image of OH LIF excited at $Q_1(5.5)$ revealing the development of the shear layers along the flamefronts for a non-acoustically forced flame (adapted from Ayoola, 2005). (Figure is provided in color online.)

bluff-body. The bluff-body created a blockage ratio of 50% and was chosen based on a scaled model of an RB211 Rolls Royce combustor (Armitage et al., 2004). For the selected flow conditions described above, three phase angles within the acoustic cycle were chosen for the generation of temperature maps. Only three were chosen, due to the large number of measurements needed for each phase angle. Nevertheless, a choice of three allows the evolution of the flame to be observed within the temperature maps. The specific phase angles are 90°, 150°, and 210°, where 0° is taken as the cross over point at which the inlet flow rises above the mean flow rate value during the sinusoidal cycle. These phase angles were chosen, because the flame structure changes the most over these three phases, as observed in the results from Ayoola et al. (2009). The CARS point measurements were taken within the measurement cross-section shown in Figure 1a, where the longitudinal axis of the probe volume was orthogonal to the measurement cross-section. This cross-section represents the maximum extent of point measurements with a height of 30 mm and a width of 20 mm. The left edge lies on the burner axis and the bottom edge is 3 mm above the bluff-body surface.

It should be noted that all the above conditions of the burner reproduce that of Ayoola et al. (2009). However, the quartz casing at the top of the burner, whose dimensions are given by Balachandran et al. (2005), was absent in this work. The casing was part of the original model burner, but needed to be removed so that CARS

measurements could be made. The curvature of the quartz casing presented a problem with regard to beam alignment. Very precise beam alignment is required, so that a CARS signal could be generated. The removal of the casing potentially presents a problem in the subsequent interpretation of temperatures from CARS measurements. Since the casing confined the flame and prevented air entrainment from the surrounding atmosphere, its removal would cause the incoming fuel/air mixture to be diluted at the outer edges. Leaner fuel/air mixtures generate lower temperatures upon burning, and this would present challenges to the valid comparison of CARS temperatures to that of URANS under confined conditions.

However, the amount of air entrainment would depend on the position in the flame. Entrainment is induced by the development of vortices at the shear layer between the atmosphere and the incoming fuel/air mixture. With increasing height from the burner there is greater vorticity at the shear layer, and this induces more mixing between the surrounding air with the fuel/air mixture. This would cause greater dilution of the mixture further up the flamefront. Figure 1b illustrates the effect of increasing vorticity with height for both the inner and outer shear layers for a non–acoustically forced flame (Ayoola, 2005). This is demonstrated indirectly by the increase in wrinkling of the flamefronts with height. This is because the vortices act to contort the flamefront. Closer to the burner, Figure 1b shows that the shear layers are more stable. This implies that the amount of air entrainment is less, and so the fuel equivalence ratio local to the flamefront there is closer to 0.55. With the aid of turbulent mixing, the burned gases close to this region would therefore exhibit temperatures closer to the adiabatic limit corresponding to an equivalence ratio of 0.55. Although this cannot be proven *a priori*, subsequent temperature measurements would confirm this if values are close to the adiabatic limit. Any air entrainment would lower the temperature noticeably, since the adiabatic temperature drops more steeply with a decrease in equivalence ratio at lean conditions (Turns, 2000). Measured temperatures close to the bluff-body in the burned gases would therefore lend themselves to a more valid comparison to URANS results under confinement. Nevertheless, all of the above argument is based on the presupposition of comparing the results from our experiments to simulations of a confined flame. Otherwise, our experimental dataset could also be used for validation studies of simulated flames under no confinement. Although the unconfined case would lend itself to more accurate comparison, our study could additionally facilitate validation of simulations under confinement whereupon boundary conditions are easier to define in the establishment of a numerical model.

Laser Diagnostics

Setup. Figure 2 shows the CARS setup to measure temperature. This comprised a frequency doubled 10 Hz-pulsed Nd:YAG laser (Surelite Continuum II-10). Using the Nd:YAG laser and frequency doubling, green light at 532 nm was emitted and this was used to pump a dye laser that emitted a red beam centered at 606 nm with a full width at half maximum (FWHM) of 6 nm. To achieve this, the dye composition was optimized to yield maximum power near 606 nm. The resulting dye composition was 1.11×10^{-4} M rhodamine 640 in ethanol.

The output of the Nd:YAG laser was split using beam samplers (BSs), where approximately 7% of the incident beam was directed into the dye laser cavity for

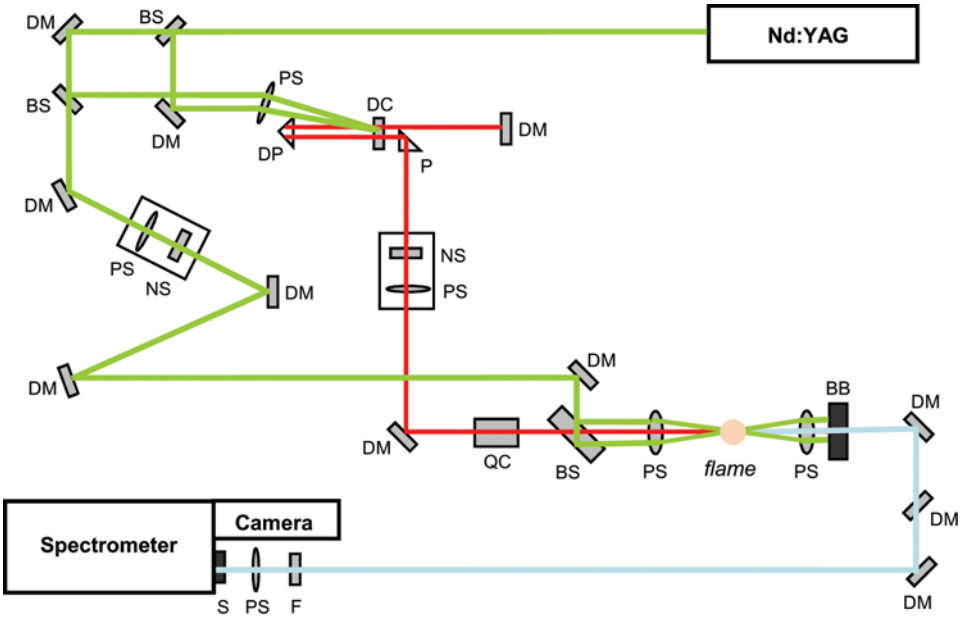

Figure 2 The CARS optical setup. Description of the components: DM – dichroic mirror; BS – beam sampler; PS – positive spherical lens; NS – negative spherical lens; DP – prism with dichroic coating; P – prism; BB – beam block; QC – quartz cylinder to adjust height of beam; F – filter; S – slit; DC – dye cell. (Figure is provided in color online.)

both the oscillator and amplifier parts of the dye laser. The remaining green beam was expanded by using a Galilean telescope and allowed the collimation of the beam to be finely tuned. The beam was also reflected to and from several dichroic mirrors (DMs), in order to create a time delay that compensated for the extra time photons spent inside the dye laser cavity, thus ensuring that the pump (532 nm) and Stokes (606 nm) beams arrived simultaneously at the measurement point during the 10 ns laser pulse. The dye laser output emitted broadband light, whose wavelength was spectrally centered at 606 nm with a FWHM of 6 nm. The output was generated by pumping both the oscillator and amplifier sections, which used a common dye cell. The Stokes beam was then expanded similarly to the pump beam, in order to match the diameters of all beams that reach the measurement volume. Both the quartz cylinder (QC) and beam splitter (BS) provide sufficient degrees of freedom to position and orient the pump and Stokes beams, in order to satisfy the folded BOXCARS phase-matching criterion; see Chrystie (2009b) for details. The three beams were then focused through a PS lens with a focal length of 290 mm, such that the beams overlap as much as possible at the measurement volume resulting in the generation of the CARS signal beam near 473 nm.

Once positioning and orienting of the beams had been achieved optimally using the PS lens, quartz cylinder, and beam splitter, all the beams were recollimated using another 290 mm PS lens. The paths of the resulting pump and Stokes beams were blocked using a beam block (BB) allowing only the CARS beam to pass. The CARS beam then passed through a dichroic mirror (DM) to filter-out the residual 532 nm

light, whereupon the beam was spectrally resolved. The filtered beam was resolved by directing it to a large spectrometer (SPEX) of length 1.2 m and instrumental resolution of 0.24 cm^{-1} at a detection wavelength of 473 nm. The spectrum was detected and recorded on a laser-triggered 14-bit back illuminated EMCCD camera (Andor iXon DV887ECS-BV). The camera offered a high quantum efficiency of 95%, thus allowing the weak CARS signals to be detected with little noise. The 512×512 pixel chip (16 μm pixel size) on the camera was capable of being cooled using an in-built Peltier system. The chip was cooled to no more than $-30°C$, which reduced the quantity of dark noise to negligible levels.

Spectral evaluation. Upon resolving the signal, a single shot spectrum was recorded on a computer. To enable proper spectral evaluation, background levels and nonresonant spectra in room-temperature propane were also recorded. These additional data are needed to compensate for background and dye laser contributions that distort the underlying CARS spectra from which temperature can be measured. The two are treated in turn. First, the background originates from visible flame emission, contribution from the camera electronics, and stray light external to the spectrometer. Each CARS spectrum was corrected for background. Acquisition of background spectra involved recording while the Stokes beam was blocked. One hundred such spectra were recorded to yield an averaged background spectrum that was subtracted from each subsequently acquired CARS spectrum. Second, each CARS spectrum must be divided by a nonresonant spectrum. This corrects for the non-uniform dye laser profile and any irregularities in the detection system, such as defective pixels on the camera chip. The nonresonant spectrum was generated by recording a CARS spectrum in propane at room temperature. Propane does not possess any resonant transitions in the wavelength region of the dye laser emission, and instead relies on the weak nonresonant processes that naturally occur simultaneously with resonant CARS processes (Eckbreth, 1996). The intensity of the propane spectrum depends only on the laser beam strength, and therefore mimics the spectral profile of the dye laser. The propane spectrum was compensated for background intensity in exactly the same manner as for the nitrogen spectrum. It should also be noted that in the correction for the non-uniform dye laser profile, the Nd:YAG laser used as the pump was not seeded and exhibited slight multimodal fluctuation. This contributed to a dye laser profile that fluctuated irregularly from shot-to-shot. Details of the effect on the data are given below in the section called "CARS Spectra." Once the correction for the overall dye laser profile had been accounted for, a computer program named CARSFT (Clark et al., 1990) was used to fit the theoretical spectra to experimentally generated ones in order to infer temperature.

Spatial resolution. The spatial resolution of the setup was also estimated, in order to ensure that thermal lengthscales could be determined with sufficient accuracy. The measurement was conducted by using a hypodermic needle that was connected to a propane source. Propane flowed from the tip of the needle (diameter of 0.5 mm), whose tip intersected orthogonally to the horizontal plane of the pump beams. The needle was then translated along the beam direction, and the CARS spectra were recorded for each needle position. The length of the measurement volume was estimated from recording the peak intensity of the CARS spectra and then noting the position from where the peak intensity subsided to half the maximum value along

the translation path. This yielded a length of approximately $L_{50\%} = 5$ mm. The diameter of the measurement volume was also estimated by considering the overlap of the beams yielding a value of approximately 100 μm. The spatial resolution here is limited by the length, $L_{50\%}$, whose value is comparably larger than typical of most folded BOXCARS configurations, being 1 mm or less (Eckbreth 1996; El-Diasty 2011). Given the constraint on laser power, being ~295 mJ/pulse, it was necessary to increase the overlap of the beams, and hence increase the measurement volume length in order to obtain more signal to compensate for the lower laser power.

RESULTS AND DISCUSSION

CARS Spectra

Figure 3 shows a match between a theoretical and an example single-shot experimental CARS spectrum measured at a typical flame temperature of 1600 K in the bluff-body burner. The least-squares fit shows a good agreement, as shown by the good overlap of the spectra, and the square of the residual; here the residual is defined as the difference between the theoretical and experimental spectra.

Although there is a good fit, the match is less than perfect as shown by the non-zero magnitudes in the plot of the square of the residual. This is caused by the dye laser spectral profile being recorded as an average, instead of simultaneously capturing the instantaneous dye laser and CARS spectra. Simultaneous capture would otherwise allow all CARS spectra to be normalized by their corresponding dye laser spectrum, thus eliminating the effect of nonperfect referencing. Nevertheless, good fits were obtained and this was reflected in the spread of temperatures

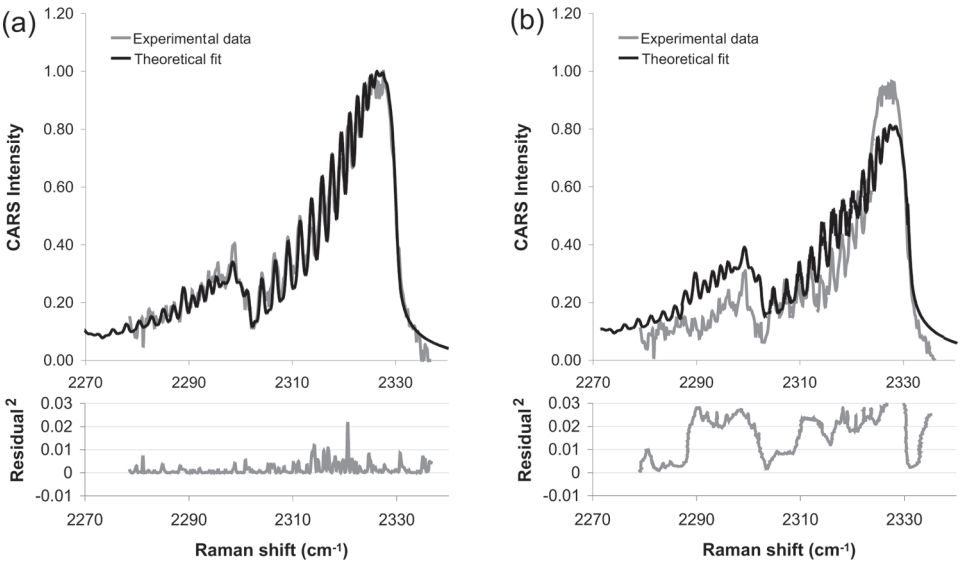

Figure 3 (a) Example match for a single-shot experimental spectrum with a theoretical one at a temperature of 1600 K in the bluff-body burner. (b) Example of an attempted fit to an experimental hybrid spectrum.

measured in a test flame. The test flame was steady, flat, and laminar, and its reactants were composed of methane and air at an equivalence ratio of one. The average temperature of the test flame was measured to be 2180 K with a FWHM spread of 92 K (4.2%). This served as a quick check of the validity of the CARS setup used here, whose temperature and precision were in close agreement with previous studies (Hartung et al., 2006; Snelling et al., 1987). Furthermore, it is possible that nonperfect referencing could introduce systematic error. This was checked by making a fit to an ensemble-averaged CARS spectrum over 100 single shot spectra and comparing the resulting temperature to the average temperature derived from the fitting of single shot spectra. In the case of the ensemble-averaged spectrum, the dye laser profile is also averaged, therefore the fitting in this case is equivalent to perfect referencing. By comparing the two methods to obtain the mean temperature, the effect of nonperfect referencing on accuracy can be investigated. Here it was found that it introduced an error of up to 0.5% at temperatures between 1400 and 1700 K.

The Acoustic Cycle

Before studying the temperature distributions in the acoustically forced flame, which were derived from the fitting of CARS spectra, a closer look at the dynamics of the flame is required to assist in the interpretation of the results.

Dynamics of the acoustically forced flame. Figure 4 shows the phase-averaged velocity flowfield and heat release rate (HRR) of the central cross-section of the flame for the three phase angles studied here at the conditions described in the figure caption. These data are from URANS simulations, as reported in Armitage et al. (2006). The cross-section is split into two panes, where the line of symmetry is the centerline at a radial position of zero. The left pane shows the velocity vector field and the progress variable (based on the fuel mass fraction) contour at a value of 0.5. The contour allows one to delineate the position of the flamefront. The right pane depicts the HRR, whose profile corresponds to the shape of the progress variable contour. Here, the shape of the HRR profile and progress variable contour represent the time-averaged position of the flamefront, and is termed the flamebrush. The images correspond to the flame conditions where the inlet velocity varies with time as shown by the plot in Figure 4. The three phase angles are also marked on the time trace for 90°, 150°, and 210°, corresponding to positions in the cycle in Armitage et al. (2006) and Ayoola et al. (2009).

It is seen in the velocity flowfield that there exist two vortices, as shown by the vectors highlighted in red in Figure 4. The top one is the main vortex, which remains in a relatively stationary position over the course of the acoustic cycle, and this forms the inner recirculation zone. The main vortex twists the upper reaches of the flamebrush down toward the burner, as shown by the rotated progress variable contour at a height of about 50 mm for the phase angle 90°. Another vortex sheds from the inlet at the beginning of the cycle and propagates upward toward the main vortex, where coalescence of the two occurs. The shedded vortex rotates in the same direction as the main vortex and twists the flamebrush down toward the burner, as shown in Figure 4. The upward flow of reactants at the inlet results in two flamefronts, one of which is stabilized on the lip of the bluff-body and separates the cold unburned gases from the region of hot burned gases in the inner recirculation zone. The

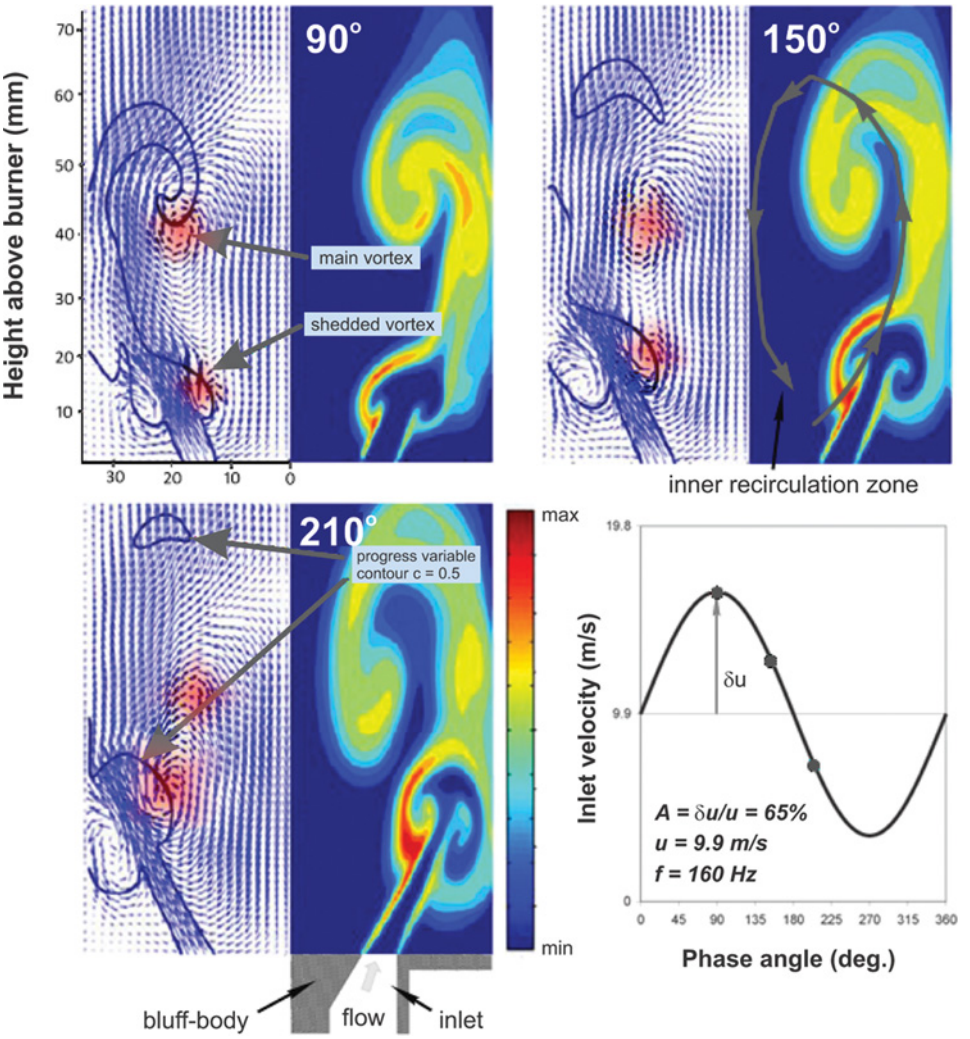

Figure 4 Depiction of phase-averaged flowfields and heat release rates (HRR) in the central cross-section of the acoustically forced flame at a forcing frequency of 160 Hz, amplitude ratio of 65%, and a mean flow velocity of 9.9 m/s for three phase angles (Armitage et al., 2006). (Figure is provided in color online.)

corresponding flamebrush is inclined and approximately straight for a certain height until it is twisted down toward the bluff-body. This flamebrush distortion is caused by the propagation of the shedded vortex that emerges from the inlet. The propagation is synchronous with the sinusoidal perturbation of the reactant flow, such that during an increase in the volumetric flowrate in the cycle a new vortex propagates upward and curls the flamebrush.

Comparison of temperatures. Figure 5 shows maps of phase-averaged temperature on the cross-section of the axisymmetric flame that was subjected to acoustic-forcing. The maps correspond to the right half of the flame in Figure 4.

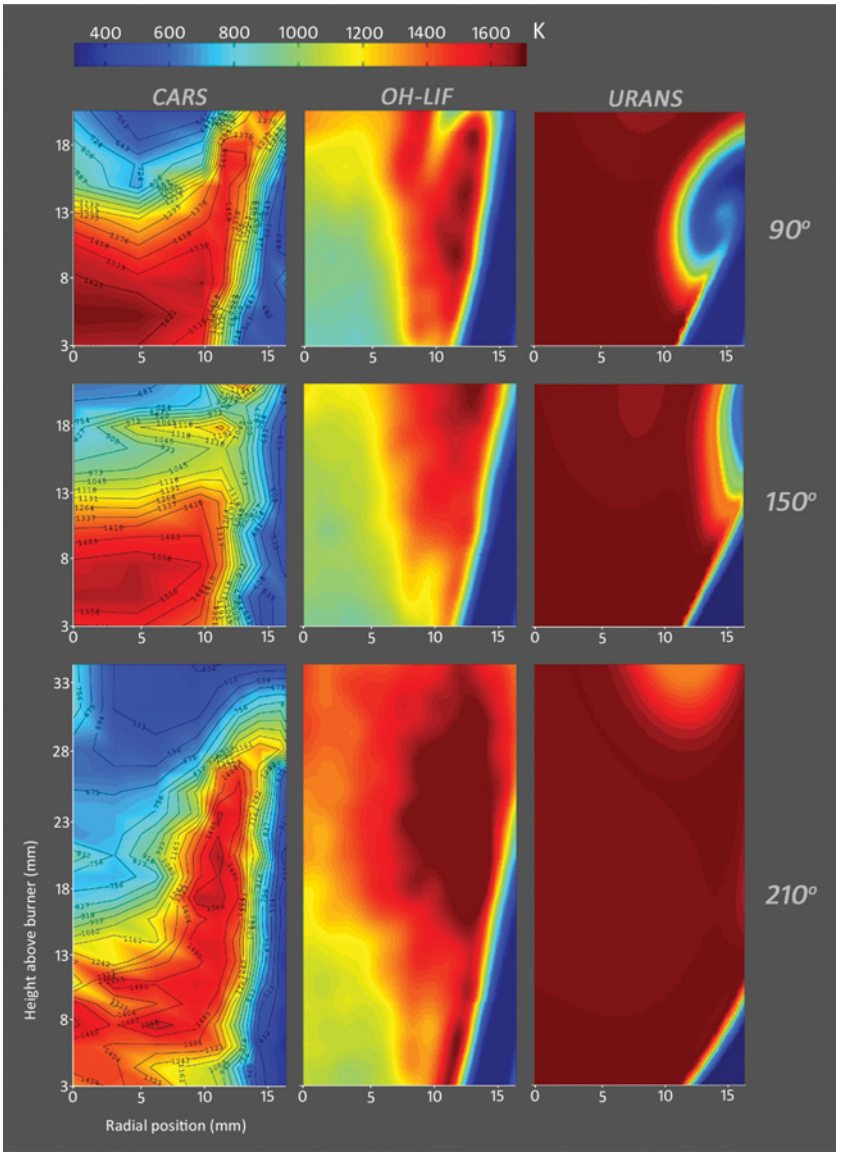

Figure 5 Phase-averaged temperature maps for the central cross-section of the flame at three phase angles. The figure consists of results from the following: left column: CARS, middle column: OH PLIF (Ayoola et al., 2009), and right column: URANS (Armitage et al., 2006). (Figure is provided in color online.)

The temperatures from the CARS technique, along with temperature maps derived from OH PLIF (Ayoola et al., 2009) and URANS (Armitage et al., 2006), are shown for the three phase angles 90°, 150°, and 210°. The left edges of the maps in Figure 5 coincide with the burner's central axis. The bottom edge of the maps is taken to be 3 mm above the burner surface, whose length comprises of two sections: a 12.5 mm radius bluff-body and a 5 mm gap from which the reactants flowed.

By comparing the temperature maps from the three techniques in Figure 5, it is clear that the steep temperature rise from right to left within each image is attributable to the presence of the flamebrush. The temperatures of the hot regions to the left of the flamebrush are in good agreement with the corresponding regions shown by URANS. However, the CARS results show that, in general, there is a gradual reduction in temperature of the order of 200 K in the hot region through the cycle from 90° to 210°. This difference in behavior through the cycle is likely to be caused by heat loss to the surroundings that is not present in the adiabatic case of URANS. Toward the beginning of the cycle at 90°, for the experimental results, the shedded vortex convects a lot of heat from the highly twisted flamebrush to the burned gases close to the bluff-body. However, later in the cycle, as the shedded vortex propagates upward and merges with the main vortex, the flowfield adopts a character more similar to the case where there is only the main vortex present. This means that in the later stages of the cycle, more of the gases from the upper reaches of the flame are convected down toward the bluff-body by the main vortex in the inner recirculation zone. Since the gases from further above are cooler due to greater levels of air entrainment at greater heights, more cooling of the burned gases close to the bluff-body occurs. This is also evident in the URANS results, albeit less so because of the adiabatic conditions, where it can be seen that a region of cooler gas migrates towards the bluff-body later in the cycle at 210°. It is also seen that there is a small region of significantly cooler gas local to the lip of the bluff-body at a height of $\sim$3 mm at a phase angle of 210° in the CARS results. This is likely to be due to local flame extinction at various instances in the recording of the phase-averaged temperature. Flame extinction would allow cooler unburned gases to escape into the region of burned gases at this point in the flame. This behavior would be consistent with the general lowering of the burned gas temperature, where the flamefront becomes more difficult to stabilize, consequently leading to spasmodic flame extinction at the bluff-body lip.

Further to the variation in overall temperature among the three phase angles, the difference in temperature between the hot regions of CARS and URANS is attributable to the adiabatic modeling assumptions of the latter. The hotter temperatures in the URANS case would result in more viscous burned gases (Linneken, 1977). This contribution would account for the slowing of the propagation rate of the shedded vortex up the flamefront, as demonstrated by the relative heights of the vortical structures for the same phases between CARS and URANS, as proposed earlier in the Introduction. As seen in Figure 5, URANS also shows a marked difference in the inclination of the flamebrush in contrast to both CARS and OH PLIF. This effect could be due to the incorrect modeling of the flow pattern in the inner recirculation zone, and its effect on the position of the flamefront. The difference in flamebrush inclination between experimental and modeling results can also be clearly seen in Armitage et al. (2006).

It is seen that there are positive temperature gradients in the vertical direction close to the bluff-body burner surface for the three phase angles in Figure 5. This is illustrated clearly in Figure 6 in which the plot shows the variation of CARS temperature with height on the axis of the burner. It is seen that there exists a positive temperature gradient close to the bluff-body surface up to about 5 mm. The positive temperature gradient indicates the conduction of heat into the bluff-body. This does

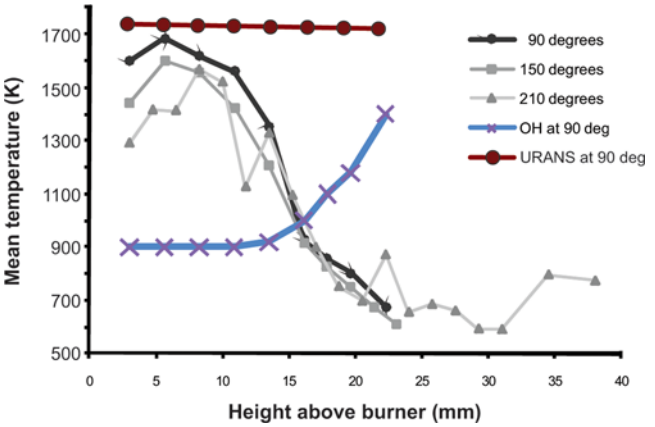

Figure 6 Phase-averaged temperatures along the centerline of the burner (i.e., radial position= 0 mm) from CARS, OH PLIF, and URANS. (Figure is provided in color online.)

not exist in the URANS case, as the model has an adiabatic boundary condition at the bluff-body surface.

Comparison of temperature profiles between the different methods reveal that OH PLIF does not also correctly predict temperature gradients close to the bluff-body surface, as shown in Figure 6 for the phase angle 90°. Interestingly, the height change over which the temperature rises to its peak along the centerline is approximately 5 mm in the CARS results. This is to within the 10 mm estimate for the thermal boundary layer, δ_{th}, discussed in Chrystie (2009b).

As discussed in the Introduction, the temperatures of the burned gases close to the bluff-body as measured using OH PLIF seemed considerably underestimated. The application of CARS clearly demonstrates this, where there is a maximum discrepancy of 800 K between the results for the phase angle 90°, as seen in Figure 6. The magnitude of the temperatures in the region together with the thickness of the thermal boundary layer make it clear that indeed conduction does occur, but not to the extent as portrayed by the large cool region in the OH PLIF results. Furthermore, the maximum temperature of the region of hot gases measured using CARS (i.e., 1691 K), as seen at the phase angle of 90°, also approaches the adiabatic flame temperature of 1706 K (Morley, 1997) for the equivalence ratio of 0.55. This suggests that the amount of air entrainment into the flame at this stage in the cycle is negligible. Therefore, the removal of the quartz casing and consequent exposure of the flame to the surrounding atmosphere has been shown not to have a significant effect on the dynamics of the flame, particularly for the early stages of the acoustic cycle. It should be noted that this effect only has a relevant consequence to the comparison of temperature data derived from our CARS experiments with that from a simulation of the bluff-body stabilized flame under confinement. The issue of confinement was discussed earlier in the section called "Burner Setup." However, for the purpose of more accurate validation of a simulated flame, it would be favorable to compare the flame studied under our conditions to a simulated flame under no confinement.

The remaining regions of the flame to be considered are the apparently cooler ones, as measured using CARS for heights above the burner in excess of 15 mm, and

as shown in Figure 5. These regions exhibit a marked decrease in temperature from the hotter region of burned gases closer to the bluff-body. This behavior is unexpected and clearly deviates from the results of OH PLIF and URANS. The reason for the deviation is thought to be caused by the presence of the fluctuating flamefront in these regions. This is illustrated in Figure 7 for the phase angle 150°, where the tip of the flamebrush that has been rotated 180° by the shedded vortex lies in the top half of the region of measured temperatures.

The implication of the fluctuation of the flamefront position in the upper regions of the burned gases is that it lowers the measured temperatures. This is the case since the spatial resolution is finite (length: 5 mm and diameter: 100 μm), and when the flamefront crosses the measurement volume, a fraction of the unburned reactants is captured. This lowers the overall temperature of the measurement volume. However the contribution to the lowering of temperature is not proportional to the fraction of the unburned gases in the measurement volume. In fact, the measured temperature is very sensitive to tiny quantities of cool gas in the measurement volume when using CARS. This point is elucidated further in the next section.

Validity of CARS Temperatures

An important aspect of the CARS results in Figure 5 is the standard deviation of temperature across all of the single measurements that constitute a

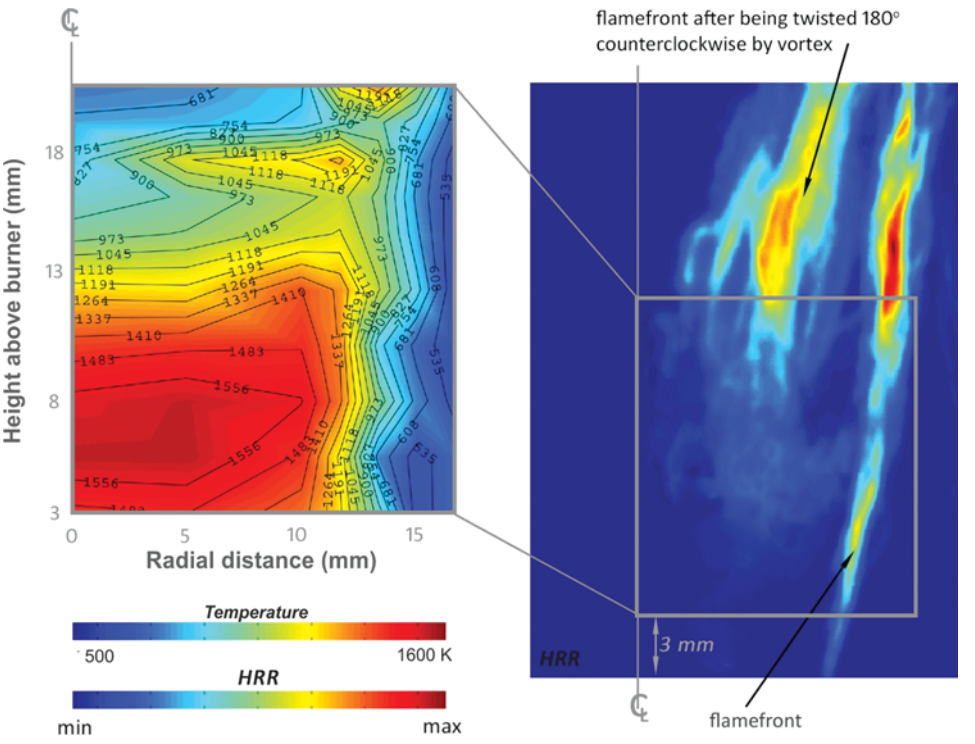

Figure 7 Comparison of HRR (Balachandran et al., 2005) to CARS temperature at a phase angle of 150° at the same flame conditions. (Figure is provided in color online.)

phase-averaged value. The standard deviation serves to help discriminate reliable temperatures. Figure 8 shows an example map of standard deviation for phase angle 90° and a corresponding phase-averaged temperature map.

Here, it is seen that regions of relatively high standard deviation correspond to lower temperatures in contrast to the region of burned gases close to the bluff-body with standard deviations to within ~100 K. The large values of standard deviation are thought to stem from the flickering of the flamefront from measurement shot-to-shot over the phase-average, as discussed earlier in relation to Figure 7. Owing to the combination of a large temperature gradient present at the flamefront and the instability in its position, any series of temperature measurements taken close to the flamefront would show a larger distribution of temperature. These measured temperatures do not necessarily represent accurately the phase-averaged temperature using the nonlinear CARS technique.

CARS results show a much cooler region in the top left of the images, which is far from agreement with URANS and OH PLIF. The relatively cool region is considered to be an artifact due to the lack of spatial resolution in the CARS experiments. When the volume is too large, it poses a problem when zones with temperature gradients are probed. This is particularly the case for probed position (c) in

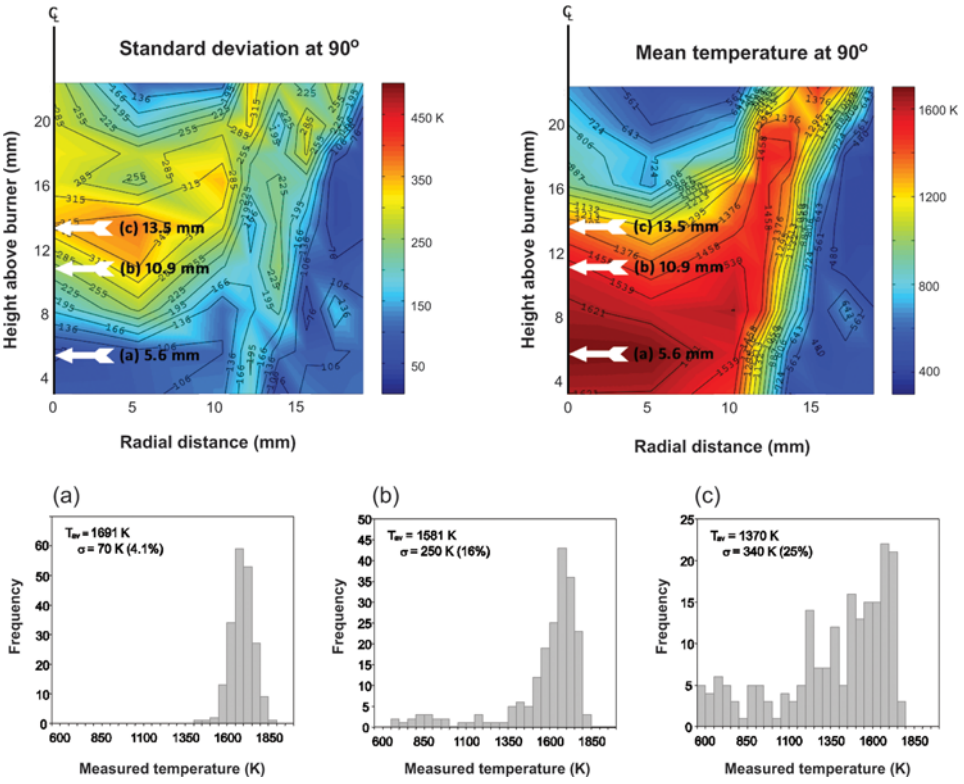

Figure 8 Standard deviation and phase-averaged temperature shown for a phase angle of 90° along with sample temperature histograms. (Figure is provided in color online.)

Figure 8, whereupon the flamebrush curls round to this position. Figure 8 also shows histograms of temperature derived from instantaneous CARS spectra for points (a), (b), and (c) within the maps of Figure 8, where it is clear that point (c), unlike (a), is not a symmetrical distribution. The combination of insufficient spatial resolution and the nonlinear nature of CARS leads to a distorted histogram. This results from the combination of spectra from the pockets of cool and hot gases within the measurement volume, which yields a "hybrid" spectrum. Due to the squared relationship between CARS signal intensity and nitrogen density, cold spectral contributions significantly outweigh the weaker hot spectra. This leads to biasing toward cooler temperatures in the hybrid spectra, and hence towards a larger spread in the distribution of temperatures and a negative skew from what would otherwise be a symmetrical distribution (Chen and Bilger, 2002; Guo et al., 2003). It is also interesting to note in this region further downstream of the bluff-body that CARS would now generally underpredict temperatures than that of OH PLIF. In spite of OH PLIF temperatures close to the bluff-body being shown to be spuriously low as outlined earlier, most likely due to a localized deficiency of OH radicals, OH PLIF measurements may be more reliable than CARS further downstream.

To resolve the problem of spatial resolution, attempts to correct for the biasing inherent in hybrid CARS spectra have been investigated previously (Boquillon et al., 1988; Parameswaran and Snelling, 1996; Seeger et al., 2006; Shepherd et al., 1990; Thumann et al., 1995). This involves accounting for the difference between the measured and true-averaged temperature of the gases within the CARS measurement volume. This essentially involves a look-up table that relates the measured temperature from the hybrid spectra to the true-averaged temperature of the measurement volume. Such a methodology could be integrated into future CFD modeling attempts, in order to better relate the dataset of this work to modeling results.

CONCLUSION

In this study, broadband vibrational nitrogen CARS was employed to provide more accurate temperature measurements in the cross-section of an axisymmetrical turbulent bluff-body premixed flame. The flame was acoustically forced and emanated from a burner, whose design is a model of a real LPP combustor. CARS spectra were recorded at several points throughout the measurement cross-section, resulting in phase-averaged temperatures. At each of the three phase angles throughout the acoustic cycle, phase-averaged temperature maps were generated by interpolating the grid of pointwise temperatures throughout the measurement cross-section. It was found qualitatively that there were significant differences between our results and that of OH PLIF by Ayoola et al. (2009). The CARS results for the burned gas regions in the flame were discriminated against for reliable temperatures by comparing the corresponding maps with maps of standard deviation. The standard deviation of the phase-averaged temperatures served to reflect the level of accuracy of the results. The primary source of inaccuracy was due to the large bias toward cooler gases present in the measurement volume, which is an inherent limitation of CARS. Despite this drawback, it was shown that the inner region of the flame above the bluff-body comprised a relatively homogeneous composition from shot-to-shot with phase-averaged temperatures of a standard deviation at a minimum of $\sim$4% at

1691 K for phase angle 90°. At this phase angle, this region was up to 47% hotter using CARS in contrast to the results of OH PLIF. The result is to be expected as this region would contain hot burned gases from the recirculation induced by the vortices emanating from the burner inlet. However, it was conceived initially that the cool regions in the results of OH PLIF were caused by the conduction of heat to the metallic bluff-body, yet the proportion of heat conducted away has been shown to be implausible. The results here show that the gases in the central region are at a temperature closer to the adiabatic limit. It has also been confirmed that conduction of heat does occur, owing to the presence of a temperature gradient close to the bluff-body surface. At a phase angle of 90°, there are regions near the bluff-body that exhibit temperatures close to the adiabatic limit of 1706 K for an equivalence ratio of 0.55. At this earlier stage in the acoustic cycle, it suggests that entrainment of air from the surrounding atmosphere into the incoming reactants is negligible in the absence of the quartz casing that had been used in previous studies of the flame. The quartz casing in our experiments had to be removed so that CARS measurements were possible. This implies that the temperatures close to the bluff-body, in the proximity of the peak temperature, are independent of the absence of the quartz casing, since the level of air entrainment is unaffected by its presence. Therefore, the CARS results for these regions, for at least the case of 90°, are deemed sufficiently accurate and hence suitable for the purpose of validating newer and more advanced versions of URANS CFD code for the model burner.

ACKNOWLEDGMENTS

The work was sponsored by the EPSRC under grant EP/F028261/1, and by Rolls-Royce plc. Dr. Robin Chrystie was supported by an EPSRC CASE studentship, whose contributions are gratefully acknowledged. Dr. Iain Burns was supported by a research fellowship from St. John's College, University of Cambridge.

REFERENCES

Ahmed, S.F., Balachandran, R., Marchionea, T., and Mastorakos, E. 2007. Spark ignition of turbulent nonpremixed bluff-body flames. *Combust. Flame*, **151**, 366.

Armitage, C.A., Balachandran, R., Mastorakos, E., and Cant, R.S. 2006. Investigation of the nonlinear response of turbulent premixed flames to imposed inlet velocity oscillations. *Combust. Flame*, **146**, 419.

Armitage, C.A., Riley, A.J., Cant, R.S., Dowling, A.P., and Stow, S.R. 2004. Flame transfer function for swirled LPP combustion from experiments and CFD. Presented at the ASME Turbo Expo., 2004-GT-53820, Vienna, Austria, July 14–17.

Ayache, S., Dawson, J.R., Triantafyllidis, A., Balachandran, R., and Mastorakos, E. 2010. Experiments and large-eddy simulations of acoustically forced bluff-body flows. *Int. J. Heat Fluid Flow*, **31**(5), 754.

Ayoola, B. 2005. Laser-based measurement of heat release rate and temperature in turbulent premixed flames. Ph.D. thesis, University of Cambridge, Department of Chemical Engineering, Cambridge, UK.

Ayoola, B., Hartung, G., Armitage, C., Hult, J., Cant, R., and Kaminski, C. 2009. Temperature response of turbulent premixed flames to inlet velocity oscillations. *Exp. Fluids*, **46**(1), 27.

Bauer, H. 2004. New low emission strategies and combustor designs for civil aeroengine applications. *Prog. Comput. Fluid Dyn.*, **4**(3), 130.

Balachandran, R., Ayoola, B.O., Kaminski, C.F., Dowling, A.P., and Mastorakos, E. 2005. Experimental investigation of the nonlinear response of turbulent premixed flames to imposed inlet velocity oscillations. *Combust. Flame*, **143**, 37.

Boquillon, J.P., Pealat, M., Bouchardy, P., Collin, G., Magre, P., and Taran, J.P. 1988. Spatial averaging and multiplex coherent anti-Stokes Raman-scattering temperature-measurement error. *Opt. Lett.*, **13**(9), 722.

Burns, I.S., Mercier, X., Wartel, M., Chrystie, R.S.M., Hult, J., and Kaminski, C.F. 2011. A method for performing high accuracy temperature measurements in low-pressure sooting flames using two-line atomic fluorescence. *Proc. Combust. Inst.*, **33**, 799.

Chen, Y.C., and Bilger, R.W. 2002. Experimental investigation of three-dimensional flame-front structure in premixed turbulent combustion—I: Hydrocarbon/air Bunsen flames. *Combust. Flame*, **131**, 400.

Chrystie, R.S.M., Burns, I.S., Hult, J., and Kaminski, C.F. 2008. On the improvement of two-dimensional curvature computation and its application to turbulent premixed flame correlations. *Meas. Sci. Technol.*, **19**, 125503.

Chrystie, R.S.M., Burns, I.S., Hult, J., and Kaminski, C.F. 2009a. High-repetition-rate combustion thermometry with two-line atomic fluorescence excited by diode lasers. *Opt. Lett.*, **34**, 2492.

Chrystie, R.S.M. 2009b. Development of novel laser diagnostic techniques for the quantitative study of premixed flames. Ph.D. thesis, University of Cambridge, Department of Chemical Engineering, Cambridge, UK.

Clark, G., Palmer, R., and Farrow, R. 1990. CARSFIT computer code, developed at Los Alamos and Sandia National Laboratories.

Dowling, A.P. 2000a. Vortices, sound and flame—a damaging combination. *Aeronaut. J.*, **104**, 105.

Dowling, A.P. 2000b. Active control of instabilities in gas turbines. Presented at the RTO VT Symposium on Active Control Technology for Enhanced Performance Operational Capabilities of Military Aircraft, Land Vehicles and Sea Vehicles, Branunschweig, Germany, RTO MP-051, May 8–11.

Eckbreth, A., and Hall, R. 1981. CARS concentration sensitivity with and without non-resonant background suppression. *Combust. Sci. Technol.*, **25**(5), 175.

Eckbreth, A. 1996. *Laser Diagnostics for Combustion Temperature and Species*. Gordon & Breach Publishers, Newark, NJ.

El-Diasty, F. 2011. Coherent anti-Stokes Raman scattering: Spectroscopy and microscopy. *Vib. Spectrosc.*, **55**(1), 1.

Guo, Z.M., Zhang, H.Q., Chan, C.K., and Lin, W.Y. 2003. Presumed joint probability density function model for turbulent combustion. *Fuel*, **82**, 1091.

Hartung, G., Hult, J., & Kaminski, C.F. 2006. A flat flame burner for the calibration of laser thermometry techniques. *Meas. Sci. Technol.*, **17**, 2485.

Hult, J., Burns, I.S., and Kaminski, C.F. 2005. Wide-bandwidth mode-hop-free tuning of extended-cavity GaN diode lasers. *Appl. Opt.*, **44**, 3675.

Lieuwen, T., Neumeier, Y., and Zinn, B.T. 1998. The role of un-mixedness and chemical kinetics in driving combustion instabilities in lean premixed combustors. *Combust. Sci. Technol.*, **135**, 193.

Linneken, H. 1977. Viscosity-temperature behaviour of gases at moderate pressure. *Forsch. Ingenieurwes.*, **43**(1), 19.

Morley, C. 1997. Gaseq: Chemical equilibria in perfect gases. Version 0.77a.

Parameswaran, T., and Snelling, D.R. 1996. Effect of spatial averaging on CARS derived temperatures. *Combust. Flame*, **106**, 511.

Seeger, T., Weikl, M.C., Beyrau, F., and Leipertz, A. 2006. Identification of spatial averaging effects in vibrational CARS spectra. *J. Raman Spectrosc.*, **37**, 641.

Seitzman, J.M., Hanson, R.K., Debarber, P.A., and Hess, C.F. 1994. Application of quantitative two-line OH planar laser-induced fluorescence for temporally resolved planar thermometry in reacting flows. *Appl. Opt.*, **33**, 4000.

Shepherd, I., Porter, F.M., and Greenhalgh, D.A. 1990. Spatial resolution of CARS in turbulent premixed combustion thermometry. *Combust. Flame*, **82**, 106.

Snelling, D., Smallwood, G., Sawchuk, R., and Parameswaren, T. 1987. Precision of multiplex CARS temperatures using both single-mode and multimode pump lasers. *Appl. Opt.*, **26**(1), 99.

Swaminathan, N., Xu, G., Dowling, A.P., and Balachandran, R. 2011. Heat release rate correlation and combustion noise in premixed flames. *J. Fluid Mech.*, **681**, 80.

Thumann, A., Seeger, T., and Leipertz, A. 1995. Evaluation of two different gas temperatures and their volumetric fraction from broadband N_2 coherent anti-Stokes Raman spectroscopy spectra. *Appl. Opt.*, **34**(18), 3313.

Turns, S. 2000. *An Introduction to Combustion*, 2nd ed., McGraw-Hill, New York.